Current status of nonhydrostatic modeling on NICAM

H. Tomita[1], M. Satoh[2], H. Miura[2], Y. Niwa[3]

[1] *Advanced Institute for Computational Science / RIKEN (htomita@riken.jp)*
[2] *Atmosphere and Ocean Research Institute/ The University of Tokyo*
[3] *Meteorological Research Institute*

ABSTRACT

NICAM (Nonhydrostatic Atmospheric ICosahedral model) is a global nonhydrostatic model for the climate study by explicit cloud expression. In the model, the fully compressible equation system is discretized by the finite volume method. To avoid the pole problem, it employs the modified icosahedral grid. The nonhydrostatic scheme developed for this model ensures the conservation of total mass and energy. The advection scheme on the icosahedral grid in NICAM is an upwind bias scheme with reduction of computational cost, having the consistency with continuity (CWC). This paper gives a summary of current status of NICAM dynamical core, focusing on numerical techniques used on it. The future direction to the exa-scale computing is also discussed.

1 Introduction

In the last decade, NICAM (Nonhydrostatic ICosahedral Atmospheric Model; Satoh et al. (2008)) has been continuously developed, aiming high-resolution global atmospheric simulations, by cooperative effort of Research Institute for Global Change / Japan Agency for Marine Science and Technology and Atmosphere and Ocean Research Institute / The University of Tokyo. This model has been employed for the pilot study of the climate research by the global cloud-system resolving approach. The first global cloud-system resolving simulation was performed by using this model(Tomita et al., 2005). Although this simulation is an aqua planet experiment, it clarified that the global cloud-system resolving approach is promising for the expression of hierarchical cloud organization and the diurnal cycle of precipitation. The subsequent paper (Nasuno et al., 2007) analyzed multi-scale cloud organization with the interaction of planetary-scale motion. An attempt for climate-sensitivity estimation by this model was also performed in the context of the aqua planet experiment(Miura et al., 2005). As the simulation with the real topography, Miura et al. (2007) successfully simulated the Madden Julian Oscillation event occurred in December 2006 and demonstrated the usefulness of global cloud-system resolving model to investigate such intra-seasonal variation. Oouchi et al. (2009,?) also performed relatively-long range simulation of several months in order to examine the major tropical phenomena, including the monsoon onset, MJO and tropical cyclone associated with it. Recently, Yamada et al. (2010) performed the first experiment in the future warmed climate by the global cloud-system resolving approach to investigate the change of tropical cyclone activity. The other NICAM activity is found in http://www.nicam.jp.

Thus, high-resolution simulations with global cloud-system resolving approach have great potential to improve the model performance and are very useful to investigate the interaction between cloud dynamics and large scale phenomena with cloud hierarchical organization. In the near future, global cloud-system resolving model will be certainly a major tool for the climate study and numerical weather forecasting. To enhance such research and forecasts, a crucial key is how we can obtain high computational-efficiency and physical-performance. In this sense, the strategy on selection of equation systems and numerical method would be very important in the nonhydrostatic modeling. In order to design the model with high efficiency, we should consider the parallelization strategy also, considering the future supercomputer architecture.

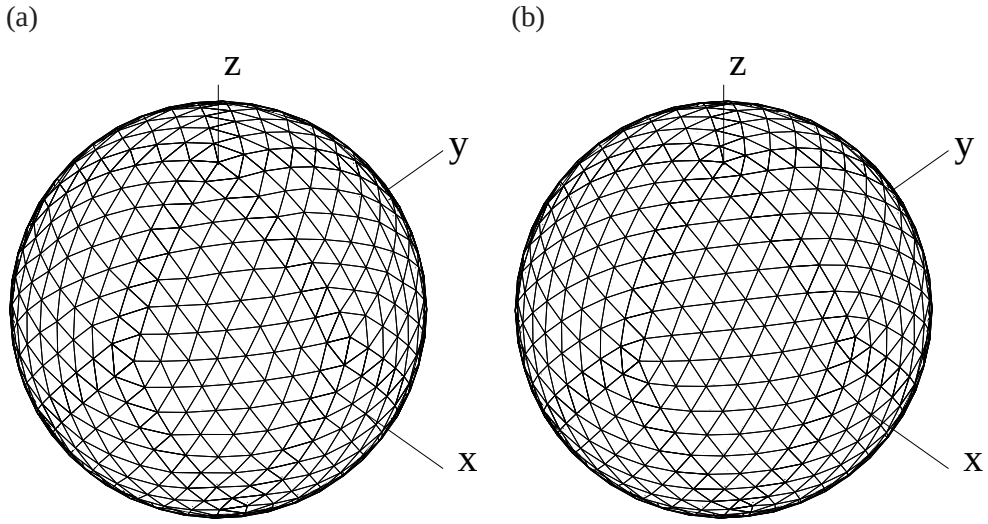

Figure 1: (a) Standard grid with glevel-3. (b) Modified grid with glevel-3.

In this paper, we review the NICAM dynamical core(Tomita and Satoh, 2004; Miura, 2007; Niwa et al., 2011), focusing on its numerical method, current problems, and future direction. In section 2 and 3, the horizontal discretization and nonhydrostatic scheme in NICAM are described, respectively. In section 4, the tracer advection scheme, which is very important for cloud, chemical, and aerosol transport, is described. Section 5 discuss the current scheme and the future direction of development. Finally, the exa-flops computing for the climate model is overlooked in section 6.

2 Horizontal discretization

2.1 Grid refinement and discretization of differential operator

The grid refinement is done by the general recursive technique which is similar to that of Stuhne and Peltier (1996). In this paper, the grid resolution obtained by l-th dividing operation is called "glevel-l", e.g., Figure 1(a) gives glevel-3 grid. All the variables are defined at the vertices of triangular grid elements. This arrangement is categorized into the Arakawa-A type grid. The control volume is defined as the polygon constructed by connecting the gravitational centers of neighboring triangular grid elements. The shape of control volume is hexagon except that it is pentagon at only twelve points inherited from the original icosahedron.

We employ the finite volume method for the discretization of differential operators. For example, the divergence operator is discretized as follows. Figure 2(a) gives the schematic figure of horizontal control volume. If a set of vectors $\mathbf{u}$ is given at all the vertices of triangles P_i, vectors $\mathbf{u}$ at the vertices of control volume Q_i are interpolated as

$$\mathbf{u}(Q_i) \simeq \frac{\alpha \mathbf{u}(P_0) + \beta \mathbf{u}(P_i) + \gamma \mathbf{u}(P_{1+mod(i,6)})}{\alpha + \beta + \gamma}, \tag{1}$$

where α, β, and γ are the areas of $Q_i P_i P_{1+mod(i,6)}$, $Q_i P_{1+mod(i,6)} P_0$, and $Q_i P_0 P_i$, respectively. The number 6 is replaced with 5 at the pentagonal control volumes. The divergence is calculated from the Gauss theorem as

$$\nabla \cdot \mathbf{u}(P_0) \simeq \frac{1}{a(P_0)} \sum_{i=1}^{6} b_i \frac{\mathbf{u}(Q_i) + \mathbf{u}(Q_{1+mod(i,6)})}{2} \cdot \mathbf{n}_i, \tag{2}$$

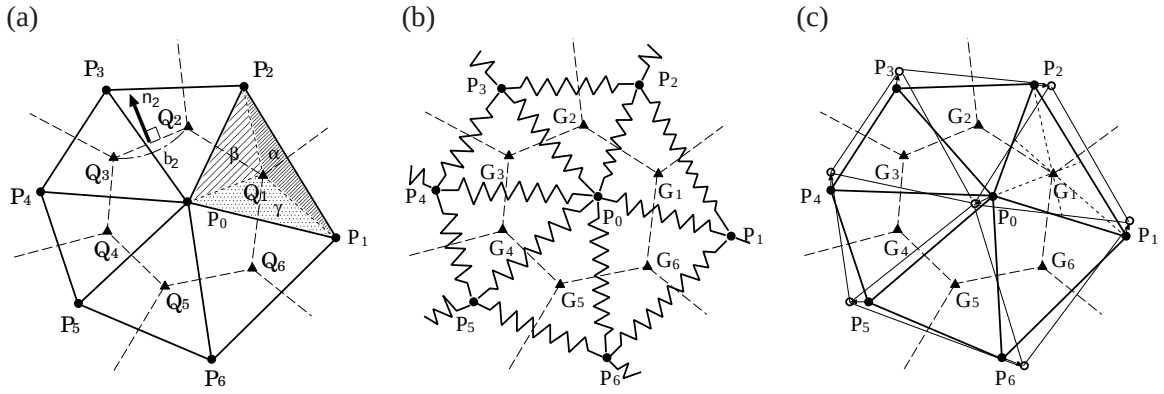

Figure 2: (a) Schematic figure of control volume. (b) Modification by the spring dynamics. (c) Modification by the gravitational center reallocation.

where b_i and $\mathbf{n}_i$ denote the geodesic arc length of $Q_iQ_{1+mod(i,6)}$ and the outward unit vector normal to this arc at the midpoint of $Q_iQ_{1+mod(i,6)}$. $a(P_0)$ is the area of control volume at the point P_0. The other differential operators such as are formulated by the similar way.

2.2 Modified icosahedral grid

The combination of the standard grid and the discretization in Eq.(2) has severe problems on the numerical accuracy and stability. Tomita et al. (2001) proposed a modification method of icosahedral grid in order to reduce the systematic grid noise and to improve the accuracy of operators. There are two steps in this method. In the first step, we apply the spring dynamics as follows; Grid points are connected by appropriate springs (Fig.2(b)). Starting from an appropriate initial condition, the equations of spring dynamics are numerically solved until the dynamical system calms down. This modification well reduces the grid-noise in the numerical integration of equations.

In the second step, the locations of gridpoints are moved to the gravitational centers of control volumes as in Fig.2(c). This modification gives second-order accuracy not only globally but also locally. One arbitrary parameter to make such a grid system is the natural length of spring. Tomita et al. (2002) examined its sensitivity to the generated grid and proposed an optimization method of the grid.

3 Nonhydrostatic framework

3.1 Governing equations

The governing equations employed in NICAM dynamical core are based on the Euler's equations without any approximation. In the traditional atmospheric models, the shallow atmosphere approximation has been used conventionally. One may point out, however, that this approximation leads to inconsistency for conservation of the absolute angular momentum unless several metric terms and the vertical Coriolis term are neglected(Phillips, 1966; Kasahara, 1974; Staniforth and Wood, 2003); if the equation of absolute angular momentum is constructed from the set of momentum equations, the global integration of the absolute angular momentum is not guaranteed for the sake of this approximation. NICAN dynamical core avoids this inconsistency by considering the deep atmosphere. We introduce a "deep"

factor :

$$\gamma \equiv r/a, \tag{3}$$

where r and a denote the distance form the center of earth and the earth radius at the sea level, respectively.

For the treatment of topography, we employ the terrain-following coordinate with the metrics as

$$\xi = \frac{z_T(z-z_s)}{z_T-z_s}, \quad G^{1/2} \equiv \left(\frac{\partial z}{\partial \xi}\right)_h, \quad \mathbf{G^z} \equiv \nabla_{h0}\xi = -\frac{\tilde{\nabla}_{h0} z}{G^{1/2}}, \tag{4}$$

where z_T and z_s are the top of the model domain and the surface height and $(\partial/\partial\xi)_h$ denotes the derivative along the vertical direction and $\tilde{\nabla}_{h0}$ denotes the spherical gradient operator along a constant ξ plane at the sea level ($r = a$).

Since $G^{1/2}\gamma^2$ is the factor of volume against the surface, we treat the prognostic variable multiplied by this factor, i.e., the perturbation density $R = (\rho - \rho_{ref})G^{1/2}\gamma^2$ (subscript ref stands for the hydrostatic reference state), the horizontal momentum $\mathbf{V}_h = \rho G^{1/2}\gamma^2 \mathbf{v}_h$, the vertical momentum $W = \rho G^{1/2}\gamma^2 w$, and the internal energy $E = \rho G^{1/2}\gamma^2 e$. The governing equations for these quantities can be written as

$$\frac{\partial R}{\partial t} + \tilde{\nabla}_{h0}\cdot\frac{\mathbf{V}_h}{\gamma} + \frac{\partial}{\partial\xi}\left(\frac{\mathbf{V}_h}{\gamma}\cdot\mathbf{G^z} + \frac{W}{G^{1/2}}\right) = 0, \tag{5}$$

$$\frac{\partial \mathbf{V}_h}{\partial t} + \tilde{\nabla}_h\frac{P}{\gamma} + \frac{\partial}{\partial\xi}\left(\mathbf{G^z}\frac{P}{\gamma}\right) = -\tilde{\mathbf{A}}_h - \tilde{\mathbf{C}}_h, \tag{6}$$

$$\frac{\partial W}{\partial t} + \gamma^2\frac{\partial}{\partial\xi}\left(\frac{P}{G^{1/2}\gamma^2}\right) + Rg = \left(-\tilde{A}_z - \tilde{C}_z\right), \tag{7}$$

$$\begin{aligned}&\frac{\partial E}{\partial t} + \tilde{\nabla}_{h0}\cdot\left(h\frac{\mathbf{V}_h}{\gamma}\right) + \frac{\partial}{\partial\xi}\left[h\left(\frac{\mathbf{V}_h}{\gamma}\cdot\mathbf{G^z} + \frac{W}{G^{1/2}}\right)\right] \\ &- \left[\mathbf{v}_h\cdot\left(\tilde{\nabla}_{h0}\frac{P}{\gamma} + \frac{\partial}{\partial\xi}\left(\mathbf{G^z}\frac{P}{\gamma}\right)\right) + w\left(\gamma^2\frac{\partial}{\partial\xi}\left(\frac{P}{G^{1/2}\gamma^2}\right) + Rg\right)\right] + Wg = \tilde{Q}_{heat},\end{aligned} \tag{8}$$

where $P = (p - p_{ref})G^{1/2}\gamma^2$ is the perturbation pressure, h enthalpy, g the gravitational acceleration, and $\tilde{Q}_{heat}$ the heating rate.

$\tilde{\mathbf{A}}(=\tilde{\mathbf{A}}_h + \tilde{A}_z\mathbf{k})$ and $\tilde{\mathbf{C}}(=\tilde{\mathbf{C}}_h + \tilde{C}_z\mathbf{k})$ are momentum advection term and Coriolis term, respectively Here, we introduce an orthogonal basis $\{\mathbf{e}_1, \mathbf{e}_2, \mathbf{e}_3\}$, which is independent of space with $\mathbf{e}_3$ being in the same direction as the angular velocity of the earth $(0, 0, \Omega)$. We define v_1, v_2, and v_3 as the components of the three-dimensional velocity $\mathbf{v}$ with regard to the basis $\mathbf{e}_1$, $\mathbf{e}_2$, and $\mathbf{e}_3$, respectively. $\tilde{\mathbf{A}}$ and $\tilde{\mathbf{C}}$ can be expressed as

$$\tilde{\mathbf{A}} \equiv \sum_{i=1}^{3}\left[\tilde{\nabla}_{h0}\cdot\left(v_i\frac{\mathbf{V}_h}{\gamma}\right) + \frac{\partial}{\partial\xi}\left[v_i\left(\frac{\mathbf{V}_h}{\gamma}\cdot\mathbf{G^z} + \frac{W}{G^{1/2}}\right)\right]\right]\mathbf{e}_i, \tag{9}$$

$$\tilde{\mathbf{C}} \equiv 2\Omega\rho G^{1/2}\gamma^2\left(-v_2\mathbf{e}_1 + v_1\mathbf{e}_2\right). \tag{10}$$

3.2 Numerical method

Since the set of governing equations we solve is the elastic system, it may contain all of the waves realized in the actual atmosphere. The acoustic waves and the high-frequency gravity waves together with the Lamb waves are contained as the fast modes. If a fully explicit method is employed to solve Eqs.(5)-(8), the time interval is severely restricted due to the vertical propagation of the acoustic waves. On the other hand, if an implicit method is employed for both in the horizontal and vertical directions,

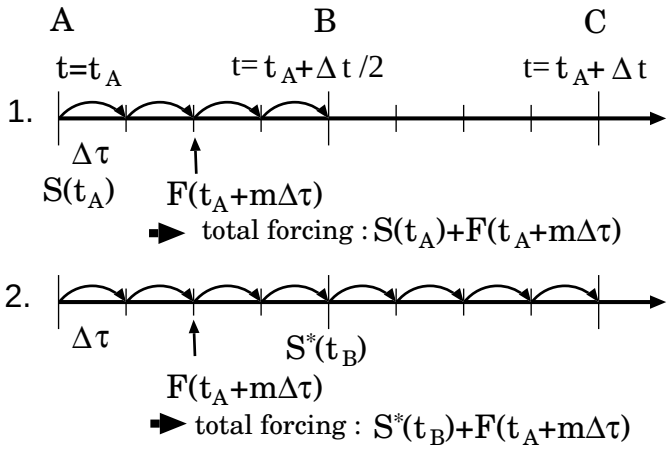

Figure 3: Schematic diagram of temporal integration.

one has to solve a three-dimensional Helmholtz equation for pressure or vertical momentum. The computational cost would be high in solving a multi-dimensional Helmholtz equation especially for high resolution simulations[1]. In order to avoid solving a multi-dimensional Helmholtz equation, we integrate the equations implicitly just in the vertical direction and explicitly in the horizontal directions. This method is called the Horizontally Explicit and Vertically Implicit scheme (HEVI). This formulation leads to one dimensional Helmholtz equation, which is easy to be solved by the direct method, because the matrix system is tridiagonal. Satoh (2002, 2003) proposed a new nonhydrostatic scheme in the context of the HEVI scheme. In order to use it for climate simulations, he formulated the scheme by taking the conservation of mass and total energy into consideration. We extend this scheme to the global domain using the icosahedral grid.

In Eqs.(5)-(8), the left-hand side terms are associated with fast propagating waves in space, while the right-hand side terms are related to relatively slow motions. We integrate the prognostic variables with the time-splitting method, namely, the fast mode terms are evaluated at every small time step $\Delta\tau$, while the slow mode terms are evaluated at larger time step Δt. For the small time step integration we use the forward-backward scheme based on the HEVI scheme, while for the large time step integration we use the second-order or third-order Runge-Kutta scheme. Figure 3 shows the time integration procedure by the second-order Runge-Kutta scheme. Let Eqs.(5)-(8) be described schematically as

$$\frac{\partial \Psi}{\partial t} - F = S, \tag{11}$$

where Ψ, F, and S represent the prognostic variable, the fast mode term, and the slow mode term, respectively. If Ψ at $t = t_A$ is known, we can evaluate the slow mode tendency $S(t_A)$. The variable is integrated from t_A to t_B by using $S(t_A) + F(t_A + m\Delta\tau)$ as the forcing at $t = t_A + m\Delta\tau$ with the fast mode tendency $F(t_A + m\Delta\tau)$ being updated at every small step, where m represents the index of small time step. Thus, the temporary value of the prognostic variable Ψ^* at t_B can be obtained. Using this value, we can evaluate the slow mode tendency $S^*(t_B)$. Returning to $t = t_A$, the variable is integrated from t_A to t_C by using $S^*(t_B) + F(t_A + m\Delta\tau)$.

The fast mode solver is the main part of dynamical core. We divide the prognostic variables into the portions at the current large step t (t_A or t_B in Fig.3) and the deviations from them. Let the value of a prognostic variable ϕ at the current large time step be ϕ^t and the deviation from it be $\phi^*(= \phi - \phi^t)$.

[1] This is still debatable. Some technique such as the multi-grid solver may resolve it or not. Anyway, it is a safe strategy to avoid the solution of multi-dimensional Helmholtz equation.

Based on the HEVI scheme, we temporally discretize Eqs.(5)-(8) by expanding the fluxes around the time t as

$$\frac{R^{*\,\tau+\Delta\tau}-R^{*\,\tau}}{\Delta\tau}+\tilde{\nabla}_{h0}\cdot\frac{\mathbf{V}_h^{*\,\tau+\Delta\tau}}{\gamma}+\frac{\partial}{\partial\xi}\left(\frac{\mathbf{V}_h^{*\,\tau+\Delta\tau}}{\gamma}\cdot\mathbf{G}^{\mathbf{z}}+\frac{W^{*\,\tau+\Delta\tau}}{G^{1/2}}\right)=$$
$$-\left[\tilde{\nabla}_{h0}\cdot\frac{\mathbf{V}_h^t}{\gamma}+\frac{\partial}{\partial\xi}\left(\frac{\mathbf{V}_h^t}{\gamma}\cdot\mathbf{G}^{\mathbf{z}}+\frac{W^t}{G^{1/2}}\right)\right], \tag{12}$$

$$\frac{\mathbf{V}_h^{*\,\tau+\Delta\tau}-\mathbf{V}_h^{*\,\tau}}{\Delta\tau}+\tilde{\nabla}_{h0}\frac{P^{*\,\tau}}{\gamma}+\frac{\partial}{\partial\xi}\left(\mathbf{G}^{\mathbf{z}}\frac{P^{*\,\tau}}{\gamma}\right)=-\left[\tilde{\nabla}_{h0}\frac{P^t}{\gamma}+\frac{\partial}{\partial\xi}\left(\mathbf{G}^{\mathbf{z}}\frac{P^t}{\gamma}\right)\right]-\tilde{\mathbf{A}}_h^t-\tilde{\mathbf{C}}_h^t, \tag{13}$$

$$\frac{W^{*\,\tau+\Delta\tau}-W^{*\,\tau}}{\Delta\tau}+\gamma^2\frac{\partial}{\partial\xi}\left(\frac{P^{*\,\tau+\Delta\tau}}{G^{1/2}\gamma^2}\right)+R^{*\,\tau+\Delta\tau}g=-\gamma^2\left[\frac{\partial}{\partial\xi}\left(\frac{P^t}{G^{1/2}\gamma^2}\right)+R^tg\right]+\left(-\tilde{A}_z^t-\tilde{C}_z^t\right), \tag{14}$$

$$\frac{E^{*\,\tau+\Delta\tau}-E^{*\,\tau}}{\Delta\tau}+\tilde{\nabla}_{h0}\cdot\left(h^t\frac{\mathbf{V}_h^{*\,\tau+\Delta\tau}}{\gamma}\right)+\frac{\partial}{\partial\xi}\left[h^t\left(\frac{\mathbf{V}_h^{*\,\tau+\Delta\tau}}{\gamma}\cdot\mathbf{G}^{\mathbf{z}}+\frac{W^{*\,\tau+\Delta\tau}}{G^{1/2}}\right)\right]+\tilde{g}^tW^{*\,\tau+\Delta\tau}$$
$$=\tilde{Q}_{heat}-\left[\tilde{\nabla}_{h0}\cdot\left(h^t\frac{\mathbf{V}_h^t}{\gamma}\right)+\frac{\partial}{\partial\xi}\left[h^t\left(\frac{\mathbf{V}_h^t}{\gamma}\cdot\mathbf{G}^{\mathbf{z}}+\frac{W^t}{G^{1/2}}\right)\right]\right]$$
$$+\frac{\mathbf{V}_h^t}{\rho^tG^{1/2}\gamma^2}\cdot\left(\tilde{\nabla}_{h0}\frac{P^t}{\gamma}+\frac{\partial}{\partial\xi}\left(\mathbf{G}^{\mathbf{z}}\frac{P^t}{\gamma}\right)\right)-\tilde{g}^tW^t, \tag{15}$$

where

$$\tilde{g}^t=g-\frac{1}{\rho^tG^{1/2}\gamma^2}\left[\gamma^2\frac{\partial}{\partial\xi}\left(\frac{P^t}{G^{1/2}\gamma^2}\right)+R^tg\right]. \tag{16}$$

The work by the pressure gradient force and the buoyancy force (the last two terms in Eq.(15)) is evaluated with Eq.(16) at the large time step. The enthalpy in the advection terms that relates to the acoustic wave speed ($c_s^2=(R_d/C_v)\,h^t$) is evaluated also at the large time step.

In small-step integration, we first solve Eq.(13) by the forward method. Using $\mathbf{V}_h^{*\,\tau+\Delta\tau}$ thus obtained, Eqs. (12), (14), and (15) can be arranged for R, W, and P as

$$\frac{R^{*\,\tau+\Delta\tau}-R^{*\,\tau}}{\Delta\tau}+\frac{\partial}{\partial\xi}\left(\frac{W^{*\,\tau+\Delta\tau}}{G^{1/2}}\right)=S_R, \tag{17}$$

$$\frac{W^{*\,\tau+\Delta\tau}-W^{*\,\tau}}{\Delta\tau}+\gamma^2\frac{\partial}{\partial\xi}\left(\frac{P^{*\,\tau+\Delta\tau}}{G^{1/2}\gamma^2}\right)+R^{*\,\tau+\Delta\tau}g=S_W, \tag{18}$$

$$\frac{P^{*\,\tau+\Delta\tau}-P^{*\,\tau}}{\Delta\tau}+\frac{R_d}{C_v}\frac{\partial}{\partial\xi}\left[h^t\left(\frac{W^{*\,\tau+\Delta\tau}}{G^{1/2}}\right)\right]+\frac{R_d}{C_v}\tilde{g}^tW^{*\,\tau+\Delta\tau}=S_P, \tag{19}$$

where we use the proportional relation between P^* and E^*:

$$E^*=\frac{C_v}{R_d}P^*. \tag{20}$$

The tendency terms in Eqs.(17)-(19) can be written as

$$S_R=-\tilde{\nabla}_{h0}\cdot\frac{\mathbf{V}_h^{*\,\tau+\Delta\tau}}{\gamma}-\frac{\partial}{\partial\xi}\left(\frac{\mathbf{V}_h^{*\,\tau+\Delta\tau}}{\gamma}\cdot\mathbf{G}^{\mathbf{z}}\right)-\left[\tilde{\nabla}_{h0}\cdot\frac{\mathbf{V}_h^t}{\gamma}+\frac{\partial}{\partial\xi}\left(\frac{\mathbf{V}_h^t}{\gamma}\cdot\mathbf{G}^{\mathbf{z}}+\frac{W^t}{G^{1/2}}\right)\right], \tag{21}$$

$$S_W=-\left[\gamma^2\frac{\partial}{\partial\xi}\left(\frac{P^t}{G^{1/2}\gamma^2}\right)+R^tg\right]+\left(-\tilde{A}_z^t-\tilde{C}_z^t\right), \tag{22}$$

$$S_P=\frac{R_d}{C_v}\tilde{Q}_{heat}-\frac{R_d}{C_v}\tilde{\nabla}_{h0}\cdot\left(h^t\frac{\mathbf{V}_h^{*\,\tau+\Delta\tau}}{\gamma}\right)-\frac{R_d}{C_v}\frac{\partial}{\partial\xi}\left[h^t\left(\frac{\mathbf{V}_h^{*\,\tau+\Delta\tau}}{\gamma}\cdot\mathbf{G}^{\mathbf{z}}\right)\right]$$
$$-\frac{R_d}{C_v}\left[\tilde{\nabla}_{h0}\cdot\left(h^t\frac{\mathbf{V}_h^t}{\gamma}\right)+\frac{\partial}{\partial\xi}\left[h^t\left(\frac{\mathbf{V}_h^t}{\gamma}\cdot\mathbf{G}^{\mathbf{z}}+\frac{W^t}{G^{1/2}}\right)\right]\right]$$
$$+\frac{R_d}{C_v}\frac{\mathbf{V}_h^t}{\rho^tG^{1/2}\gamma^2}\cdot\left(\tilde{\nabla}_{h0}\frac{P^t}{\gamma}+\frac{\partial}{\partial\xi}\left(\mathbf{G}^{\mathbf{z}}\frac{P^t}{\gamma}\right)\right)-\frac{R_d}{C_v}\tilde{g}^tW^t. \tag{23}$$

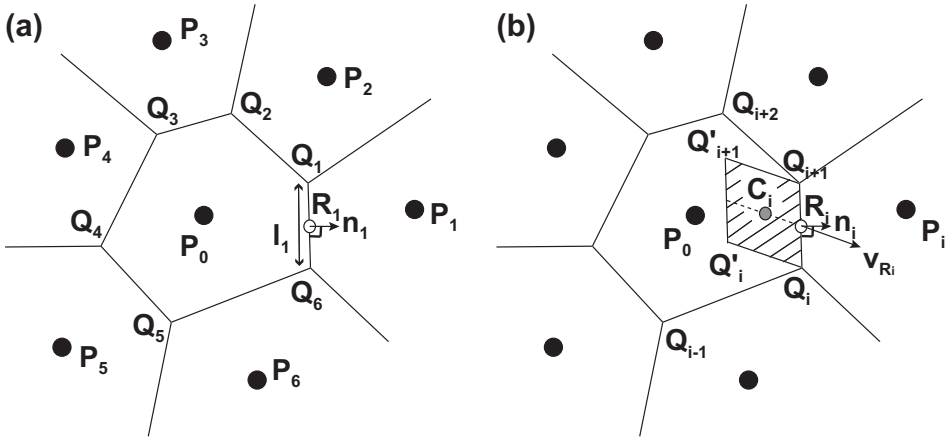

Figure 4: Schematic diagram for the upwind bias scheme on the hexagonal cell

Combination of Eqs.(17)-(19) gives the one-dimensional Helmholtz equation for W as

$$-\frac{\partial}{\partial\xi}\left[\frac{1}{G^{1/2}\gamma^2}\frac{\partial}{\partial\xi}\left(\Delta\tau^2\frac{R_d}{C_v}h^t\frac{W^{*\,\tau+\Delta\tau}}{G^{1/2}}\right)\right]-\left[\frac{\partial}{\partial\xi}\left(\Delta\tau^2\frac{R_d}{C_v}\tilde{g}\frac{W^{*\,\tau+\Delta\tau}}{G^{1/2}\gamma^2}\right)+\Delta\tau^2\frac{g}{\gamma^2}\frac{\partial}{\partial\xi}\left(\frac{W^{*\,\tau+\Delta\tau}}{G^{1/2}}\right)\right]$$
$$+\quad\frac{1}{\gamma^2}W^{*\,\tau+\Delta\tau}=\frac{W^{*\,\tau}+\Delta\tau S_W}{\gamma^2}-\Delta\tau\frac{\partial}{\partial\xi}\left[\frac{1}{G^{1/2}\gamma^2}\left(P^{*\,\tau}+\Delta\tau S_P\right)\right]-\frac{\Delta\tau}{\gamma^2}\left(R^{*\,\tau}+\Delta\tau S_R\right)g. \tag{24}$$

$W^{*\,\tau+\Delta\tau}$ and $R^{*\,\tau+\Delta\tau}$ are obtained by solving Eqs.(24) and (17), respectively.

For the evaluation of internal energy $E^{*\,\tau+\Delta\tau}$, Satoh (2002, 2003) proposed several schemes from the viewpoint of conservation; the "non-correction method" that does not consider the conversion of internal and kinetic energies, the "correction method" that modifies the conversion term between the two energies by deliberately choosing the discretization of the work done by the pressure gradient force, and the "conservation method" that perfectly guarantees the sum of the two energies by solving its flux form equation. He compared the physical performance as well as the computational performance between these schemes and concluded that the "conservation method" is the best. In this method, the conservation of total energy is guaranteed by solving the flux form equation of the total energy:

$$\frac{E_{tot}^{\tau+\Delta\tau}-E_{tot}^{\tau}}{\Delta\tau}+\tilde{\nabla}_{h0}\cdot\left[(h+\Phi+k)^t\frac{\mathbf{V}_h^{*\,\tau+\Delta\tau}}{\gamma}\right]$$
$$+\frac{\partial}{\partial\xi}\left[(h+\Phi+k)^t\left(\frac{\mathbf{V}_h^{*\,\tau+\Delta\tau}}{\gamma}\cdot\mathbf{G}^{\mathbf{z}}+\frac{W^{*\,\tau+\Delta\tau}}{G^{1/2}}\right)\right]=\tilde{Q}_{heat}, \tag{25}$$

where $\Phi(=gz)$ is the potential energy, $k(=\mathbf{v}\cdot\mathbf{v}/2)$ is the kinetic energy, and $E_{tot}=E+\rho G^{1/2}\gamma^2(\Phi+k)$. Since $\left[\rho G^{1/2}\gamma^2(\Phi+k)\right]^{\tau+\Delta\tau}$ is known, $E^{\tau+\Delta\tau}$ can be calculated by

$$E^{\tau+\Delta\tau}=E_{tot}^{\tau+\Delta\tau}-\left[\rho G^{1/2}\gamma^2(\Phi+k)\right]^{\tau+\Delta\tau}. \tag{26}$$

The deviation $E^{*\,\tau+\Delta\tau}$ is derived from

$$E^{*\,\tau+\Delta\tau}=E^{\tau+\Delta\tau}-E^t. \tag{27}$$

The more detail formulation of this method is described in Tomita and Satoh (2004); Satoh et al. (2008).

4 The advection scheme and consistency with continuity

The time evolution of tracer is given as

$$\frac{\partial}{\partial t}(\rho q)+\nabla\cdot(\rho q\mathbf{v})=0 \tag{28}$$

Note that the metric term for the topography is omitted in this section for simplicity. In the original version of NICAM, the tracer advection scheme is the same as one in the continuity equation. That is, the horizontal divergence operator of Eq.(2) is used. Although this scheme has the second order accuracy, the dispersion error is large and many spurious ripples appear consequently. In order to reduce this error, Miura (2007) developed a third order upwind scheme on the icosahedral grid. Even on the distorted hexagonal-pentagonal grid, this scheme ensures at least second order accuracy. Conceptually, this scheme is based on the val Leer's scheme I for estimation of the mass flux on the cell boundaries. Figure 4 gives the schematic diagram of this scheme. As in Fig.4(b), the mass flux passing through the edge $\mathbf{Q}_i\mathbf{Q}_{i+1}$ during one time step is estimated as the integration of quantity in the parallelogram (rectangle) $\mathbf{Q}_i'\mathbf{Q}_{i+1}'\mathbf{Q}_i\mathbf{Q}_{i+1}$. The total amount of flux passing through the edge $\mathbf{Q}_i\mathbf{Q}_{i+1}$ during the time step Δt is approximated by the amount of a tracer inside the rectangle:

$$\left(l_i \rho_{\mathbf{R_i}} q_{\mathbf{R_i}} \mathbf{v}_{\mathbf{R}_i}^{t+\Delta t} \cdot \mathbf{n_i}\right) \Delta t = \int_{S_i} \rho q dS \tag{29}$$

The distribution of quantities in the cell is expressed by the linear distribution using the gradient operator. With some algebraic calculation, these assumptions drastically reduce the computational cost without degradation of accuracy. For example, the averaged q during the time step at the center of cell edge can be expressed as

$$q_{R_i} = q_{C_i} = q_0 + (\nabla q)_{\mathbf{P_0}} \cdot (\mathbf{C_i} - \mathbf{P_0}) \,. \tag{30}$$

To guarantee the perfect monotonicity, the flux limiter developed by Thuburn (1996) is applied.

The extension of this scheme to the thee dimension is very tight work and it would spoil the virtue of less computational cost of this scheme. Therefore, NICAM applies the scheme just in the horizontal direction and employs the central difference scheme in the vertical direction with the flux limiter.

However, if we calculate both of the advection terms at the same time, the monotonicity is no longer ensured. So, NICAM employs the directional-splitting method dividing into the horizontal and vertical advection. At this moment, we must take care of the consistent way of the tracer advection scheme with the continuity equation, so-called consistency with continuity (CWC) condition. In order to satisfy the CWC condition on this method, Niwa et al. (2011) extended the intermediate density method (Easter, 1993) to the icosahedral grid. To avoid the directional bias, the following three step are applied;

1. The vertical advection process during the first $\Delta t/2$

$$Q^{\mathrm{I}} = Q^t - \frac{\Delta t}{2}\left[\frac{\tilde{q}^t_{k+1/2}\tilde{W}^*_{k+1/2} - \tilde{q}^t_{k-1/2}\tilde{W}^*_{k-1/2}}{\Delta z_k}\right] \tag{31}$$

$$\rho^{\mathrm{I}} = \rho^t - \frac{\Delta t}{2}\left[\frac{\tilde{W}^*_{k+1/2} - \tilde{W}^*_{k-1/2}}{\Delta z_k}\right] \tag{32}$$

$$q^{\mathrm{I}} = Q^{\mathrm{I}}/\rho^{\mathrm{I}} \tag{33}$$

2. The horizontal advection process during the Δt using the Miura (2007)'s scheme.

$$Q^{\mathrm{II}} = Q^{\mathrm{I}} - \frac{\Delta t}{A}\sum_{i=1}^{6}\left(l_i \hat{q}_i^{\mathrm{I}} \hat{\mathbf{V}}_i^* \cdot \mathbf{n}_i\right) \tag{34}$$

$$\rho^{\mathrm{II}} = \rho^{\mathrm{I}} - \frac{\Delta t}{A}\sum_{i=1}^{6}\left(l_i \hat{\mathbf{V}}_i^* \cdot \mathbf{n}_i\right) \tag{35}$$

$$q^{\mathrm{II}} = Q^{\mathrm{II}}/\rho^{\mathrm{II}} \tag{36}$$

$$Q^{t+\Delta t} = Q^{\mathrm{II}} - \frac{\Delta t}{2}\left[\frac{\tilde{q}^{\mathrm{II}}_{k+1/2}\tilde{W}^*_{k+1/2} - \tilde{q}^{\mathrm{II}}_{k-1/2}\tilde{W}^*_{k-1/2}}{\Delta z_k}\right] \tag{37}$$

3. The vertical advection process during the last $\Delta t/2$.

$$\rho^{t+\Delta t} = \rho^{\mathrm{II}} - \frac{\Delta t}{2}\left[\frac{\tilde{W}^*_{k+1/2} - \tilde{W}^*_{k-1/2}}{\Delta z_k}\right] \tag{38}$$

$$q^{t+\Delta t} = Q^{t+\Delta t}/\rho^{t+\Delta t} \tag{39}$$

In the above processes, the mass flux are time-averaged during the large time step, i.e.,

$$\hat{\mathbf{V}}_i^* \equiv \frac{1}{\Delta t}\sum_{n=0}^{N_s-1}\left(\hat{\rho}_i^{t+n\Delta\tau}\hat{\mathbf{v}}_i^{t+n\Delta\tau}\Delta\tau\right) = \frac{1}{N_s}\sum_{n=0}^{N_s-1}\left(\hat{\rho}_i^{t+n\Delta\tau}\hat{\mathbf{v}}_i^{t+n\Delta\tau}\right) \tag{40}$$

$$\tilde{W}_{k\pm1/2}^* \equiv \frac{1}{\Delta t}\sum_{n=0}^{N_s-1}\left(\tilde{\rho}_{k\pm1/2}^{t+n\Delta\tau}\tilde{w}_{k\pm1/2}^{t+n\Delta\tau}\Delta\tau\right) = \frac{1}{N_s}\sum_{n=0}^{N_s-1}\left(\tilde{\rho}_{k\pm1/2}^{t+n\Delta\tau}\tilde{w}_{k\pm1/2}^{t+n\Delta\tau}\right), \tag{41}$$

The use of time-averaged mass flux is crucial to satisfy the CWC condition. We can easily understand that the combination of Eq.(32), (35), and (38) are perfectly same as the discretization of continuity equation.

5 Discussion

In this paper, we summarize the current status of NICAM dynamical core. The horizontal discretization is the second order finite volume method with modified icosahedral grid(Tomita et al., 2001, 2002). The developed nonhydrostatic scheme conserves the total mass and energy(Satoh, 2002, 2003). The tracer advection by the upwind bias scheme ensures the second order accuracy not only globally but also locally(Miura, 2007). To satisfy the consistency with continuity, the techniques combined time-averaged mass flux and intermediate density is used(Niwa et al., 2011).

NICAM dynamical core is now in the mature stage as the first-generation version. As described in section 1, many fruitful results have been obtained by this model. However, during those experiments, we also found several problems, which should be overcome in the second-generation version of NICAM. The most concern is on the vertical discretization. NICAM is now employing the terrain-following coordinate. As pointed out in many literature, the pressure gradient force error becomes larger if the horizontal resolution increases. In the regional model, this problem is not so severe because the actual field does not so differ from the reference hydrostatic state. On the other hand, the difference from the reference state in the global model is larger than in the regional model. This leads to the large error of the pressure gradient force at the steep topography and occasionally the model blows up due to this error. Since the steepness of the mountain becomes severer at the higher resolution, we are insisted to change the vertical coordinate from the terrain-following coordinate to the height-based coordinate (e.g. Yamazaki and Satomura (2010)). The Arakawa-A grid in the horizontal direction that we employ with the spring grid has no fatal problem. The A-gird is free from the computational mode that appears when the degrees of freedom for mass and momentum are different. The implementation and parallelization are simpler than other grid types. However, it is also true that there remains the problem for the geostrophic adjustment with short wavelength. The change of other grid type is controversial in the near future in NICAM development.

6 Toward the exa-scale computing

Since NICAM was designed so as to bring out the high performance of massively parallel supercomputers in the high resolution simulation. it has good computational performance at this moment. Toimta et al. (2008) examined the computational performance on the Earth Simulator, which is a vector-parallel machine, and confidently remarked that the approach has enough potential to obtain the scalability on the future massive parallel machine.

The basic idea of the approach in NICAM dynamical core is the use of icosahedral grid to avoid the pole problem and horizontal explicit method to avoid the possibility of increase of iteration process

in the implicit method. From the viewpoint of the algorithm, this idea essentially does not degrade the computational performance in the future massive parallel machine. However, recent trend of the hardware is now in the transition phase and is not always optimistic for the geophysical application. The assumed problems toward the exa-scale computing are as follows:

- Memory band width problem
  Many cores are implemented in one CPU, so that the peak performance becomes tremendously high. On the other hand, increase of memory band width is slow, comparing to the CPU power. In order to obtain high performance on the scalar CPU, the efficient use of cash memory is necessary.

- Hybrid architecture
  To realize the exa-scale machine, it may be impossible to use only general-purpose chips. The help of the accelerator such as GPU may be needed. At the same time, there is a possibility of hybrid architecture of accelerator and general-purpose chip. This may insist on complicated programming to model developers. The compiler and middle-ware for reduction of this hard-work is needed.

- Network bottleneck
  The inner network is the most anxious concern for the scalability. Its speed is a crucial issue. The network topology is also important. The torus type of topology seems to be better for the gridpoint method.

- Fault tolerance
  The increase of number of CPUs causes to the increase of failure rate. It is unrealistic to frequently output restart files during the calculation. One remedy is to duplicate a memory image even on another computer node and allocate the memory image to a backup node immediately at the node failure. However, it is very hard for the application programmer to be insisted on such implementation. Middle-ware to provide the mechanism without such awareness is required.

The design of exa-scale computer is not yet clear and still debatable. To overcome the above undesirable problems, much more communication between the meteorology/climate simulation community and computer scientists are necessary.

References

Easter, R. C. (1993). Two modified versions of bott's positive-definite numerical advection scheme. *Mon. Wea. Rev. 121*, 297–304.

Kasahara, A. (1974). Various vertical coordinate systems used for numerical weather prediction. *Mon. Wea. Rev. 102*, 509–522.

Miura, H. (2007). An upwind biased conservative scheme for spherical hexagonal-pentagonal grids. *Mon. Wea. Rev. 135*, 4038–4044.

Miura, H., M. Satoh, T. Nasuno, , A. T. Noda, and K. Oouchi (2007). A Madden-Julian oscillation event realistically simulated by a global cloud-resolving model. *Science 318*, 1763–1765.

Miura, H., H. Tomita, T. Nasuno, S. Iga, M. Satoh, and T. Matsuno (2005). A climate sensitivity test using a global cloud resolving model under an aqua planet condition. *Geophys. Res. Lett. 32*, L19717,doi:10.1029/2005GL023672.

Nasuno, T., H. Tomita, S. Iga, H. Miura, and M. Satoh (2007). Multiscale organization of convection simulated with explicit cloud processes on an aquaplanet. *J. Atmos. Sci. 64*, 1902–1921.

Niwa, Y., H. Tomita, M. Satoh, and R. Imasu (2011). A three-dimensional icosahedral grid advection scheme preserving monotonicity and consistency with continuity for atmospheric tracer transport. *J. Meteor. Soc. Japan in press*.

Oouchi, K., A. Noda, M. Satoh, H. Miura, H. Tomita, T. Nasuno, and S. Iga (2009). A simulated preconditioning of typhoon genesis controlled by a boreal summer madden-julian oscillation event in a global cloud-system-resolving model. *SOLA 5*, 065–068.

Oouchi, K., A. T. Noda, M. Satoh, B. Wang, S.-P. Xie, H. Takahashi, and T. Yasunari (2009). Asian summer monsoon simulated by a global cloud-system-resolving model: Diurnal to intra-seasonal variability. *Geophys. Res. Lett. 36*, L11815.

Phillips, N. A. (1966). The Equations of Motion for a Shallow Rotating Atmosphere and the "Traditional Approximation". *J. Atmos. Sci. 23*, 626–628.

Satoh, M. (2002). Conservative scheme for the compressible non-hydrostatic models with the horizontally explicit and vertically implicit time integration scheme. *Mon. Wea. Rev. 130*, 1227–1245.

Satoh, M. (2003). Conservative scheme for a compressible non-hydrostatic model with moist processes. *Mon. Wea. Rev. 131*, 1033–1050.

Satoh, M., T. Masuno, H. Tomita, H. Miura, T. Nasuno, and S. Iga (2008). Nonhydrostatic icosahedaral atmospheric model (NICAM) for global cloud resolving simulations. *J. Comput. Phys., the special issue of Predicting Weather, Climate and Extreme Events 227*, 3486–3514.

Staniforth, A. and N. Wood (2003). The Deep-Atmosphere Euler Equations in a Generalized Vertical Coordinate. *Mon. Wea. Rev. 131*, 1931–1938.

Stuhne, G. R. and W. R. Peltier (1996). Vortex Erosion and Amalgamation in a New Model of Large Scale Flow on the Shere. *J. Comput. Phys. 128*, 58–81.

Thuburn, J. (1996). Multidimensional flux-limited advection schemes. *J. Comput. Phys. 23*, 74–83.

Toimta, H., K. Goto, and M. Satoh (2008). A new approach of atmospheric general circulation model - global cloud resolving model nicam and its computational performance -. *SIAM, J. Sci. Comput. 30*, 2755–2776.

Tomita, H., H. Miura, S. Iga, T. Nasuno, and M. Satoh (2005). A global cloud-resolving simulation: Preliminary results from an aqua planet experiment. *Geophys. Res. Lett. 32*, L08805, doi:10.1029/2005GL022459.

Tomita, H. and M. Satoh (2004). A new dynamical framework of nonhydrostatic global model using the icosahedral grid. *Fluid Dyn. Res. 34*, 357–400.

Tomita, H., M. Satoh, and K. Goto (2002). An Optimization of the Icosahedral Grid Modified by Spring Dynamics. *J. Comput. Phys. 183*, 307–331.

Tomita, H., M. Tsugawa, M. Satoh, and K. Goto (2001). Shallow Water Model on a Modified Icosahedral Geodesic Grid by Using Spring Dynamics. *J. Comput. Phys. 174*, 579–613.

Yamada, Y., K. Oouchi, M. Satoh, H. Tomita, and W. Yanase (2010). Projection of changes in tropical cyclone activity and cloud height due to greenhouse warming: global cloud-system-resolving approach. *Geophys. Res. Lett. 37*, L07709.

Yamazaki, H. and T. Satomura (2010). Nonhydrostatic atmospheric modelling using a combined cartesian grid. *Mon. Wea. Rev. 138*, 3932–3945.